The wet and dry strength variation tests showed low variations (less than 10%) for a number of blends. This indicates that there is little deterioration in strength from a dry to a saturated condition.

The grading limits of all crushed brick blends with up to 30% crushed brick content were found to be within Melbourne Water upper and lower bound grading curves for "Grade A" and "Grade B" backfill and bedding material. The crushed brick blends satisfied all Melbourne Water requirements for both Grade A and Grade B materials except the Los Angeles Abrasion requirements for Grade A material, where further testing of different blends is recommended.

6 ACKNOWLEDGEMENT

The authors would like to acknowledge Sustainability Victoria for funding this research project (Contract No: 3887). The authors would also like to acknowledge Alex Fraser Group and Delta Group for providing samples of crushed brick and crushed concrete as well as their technical assistance on this project.

The authors wish to thank VicRoads for permission to publish this paper. The views expressed are those of the authors and do not necessarily represent those of VicRoads

7 REFERENCES

Australian Standards AS 1141(1996) Method for sampling and testing aggregates, *Standards Australia, Standards* Association of Australia.

Australian Standards AS 1289 (1998) Method of testing soils for engineering purposes, *Standards Australia, Standards Association of Australia.*

Melbourne Water (2001) Sands, Crushed rock and crushed scoria, *Specification 21.A.038,* August.

Lay, M.G. (1998) Handbook of road technology, Third edition, Volume 1, Gordon and breach science publishers, The Netherlands.

VicRoads (1995) Standard Specifications for Road works and Bridge works, *Section 304, Flexible pavement construction,* February.

VicRoads (2007) Standard Specifications for Road works and Bridge works, *Section 820 Recycled crushed concrete for pavement subbase and light duty base,* January.

NUMERICAL SIMULATION OF SOFT GROUND IMPROVED WITH CEMENT

D. S. Liyanapathirana[1], M. D. Liu[2] and J. P. Carter[3]
[1]*School of Engineering, University of Western Sydney, NSW 1797*
[2] *School of Civil and Environmental Engineering, University of New South Wales, NSW 2052*
[3] *Faculty of Engineering and Built Environment, University of Newcastle, Newcastle, NSW 2308*

ABSTRACT

This paper examines, using a numerical model based on the finite element method, the undrained bearing capacity of shallow circular footings on soft ground improved with deep cement mixing. Guidelines are given to identify the importance of the degree of cementation on the bearing capacity of shallow footings. Using a bearing capacity improvement factor, the influence of the degree of cementaton and the extent of the cemented region on bearing capacity has been investigated. Finally, the performance of deep cement-mixed columns has been investigated using the numerical model. The results indicate that there exists an optimum length to diameter ratio for the deep mixed cement columns and this optimum ratio depends on the degree of cementation of the soil.

1 INTRODUCTION

During the past few decades, construction activities have increased considerably over soft ground such as around river estuaries, low-lying marshy areas and harbour foreshores, i.e., areas which may previously have been considered unsuitable for development. Due to generally low bearing capacity and often excessive settlement of these soils, geotechnical engineers dealing with footing construction over soft ground encounter a real challenge. Although consolidation-based ground improvement methods such as preloading and vertical drains are used for soft ground improvement, it is often not economical to allow the soil to gain strength and stiffness through consolidation alone due to time constraints and the uncertainty of soil conditions. As a result, a wide range of ground improvement methods has been developed to support foundations on soft ground. One such method is *in situ* deep cement mixing, which provides improved strength and reduced compressibility for soft ground (e.g., Kamon and Bergado, 1991). Due to its low cost and efficiency, this method is now increasingly used to improve soft ground.

At the laboratory scale, the influence of cementation on soft clay behaviour has been studied by Kasama *et al.* (2000), Miura *et al.* (2001), Bergado *et al.* (2004), and Hopibulsuk *et al.* (2004, 2005) and significant progress has been made in understanding the fundamental behaviour of cemented clays. Recently Liu *et al.* (2006) proposed a constitutive model for cemented clay as an extension of the Structured Cam Clay model proposed previously by Liu and Carter (Liu and Carter, 2002; Carter and Liu, 2005). This model has been successfully applied to investigate the influence of the structure of natural soils on foundation behaviour (Liyanapathirana *et al.*, 2003a, 2003b; Liyanapathirana and Carter, 2005). It has also been used successfully to describe the behaviour of cemented clay observed during laboratory experiments. Although the finite element method has been used to study the application of deep mixed columns in different geotechnical applications (e.g., Han and Gabr, 2002; Dong *et al.* 2004), use of a rigorous constitutive model capturing the salient features of cemented soil behaviour has not yet been achieved. Han and Gabr (2002) used a Mohr-Coulomb model and Dong *et al.* (2004) used a Drucker-Prager model to simulate cement-mixed soil behaviour in their finite element analyses.

The main objective of this paper is to examine the significance of the degree of cementation and the extent of the cemented region on the undrained bearing capacity of shallow footings resting on deep cement-mixed clay deposits. The influence of the degree of cementation on the load carrying capacity of deep cement-mixed columns is also investigated. A series of numerical simulations has been carried out by incorporating the constitutive model proposed by Liu *et al.* (2006) for cemented soils into the finite element program AFENA (Carter and Baalam, 1995). The new cemented clay model is a relatively simple elastoplastic model, which was developed with the aim of providing a practical tool for solving boundary value problems encountered in geotechnical engineering practice in cases where cemented soils are involved.

Based on these numerical simulations, guidelines are provided to identify the influence of the degree of cementation and the extent of the cemented region on the bearing capacity of shallow circular foundations, and the optimum length to diameter ratio for deep cement-mixed columns.

2 NUMERICAL MODEL

The axisymmetric finite element mesh used for the analysis consists of eight-node quadrilateral elements and the numerical integration was carried out using four-point Gauss integration. The mesh used for the shallow foundation analysis extends 7B in the vertical and radial directions, where B is the diameter of the footing. In both radial and vertical directions, the finite element mesh was made coarser with increasing distance from the footing.

The constitutive behaviour of the cement-mixed soil was modelled using the cemented clay model developed by Liu *et al.* (2006). The soil surrounding the deep cement-mixed columns was assumed to be in an undisturbed natural state and was modelled using the Structured Cam Clay model of Liu and Carter (Liu and Carter, 2002; Carter and Liu, 2005), which takes into account the natural structure possessed by the *in situ* soil. The footing was assumed to be rough and rigid and resting on the surface of the finite layer of soil. The footing was loaded by specifying uniform vertical displacements, which were applied incrementally to the soil beneath the footing while the rest of the top boundary of the soil layer was free to move in both radial and vertical directions. The bottom and vertical boundaries were constrained from moving in both vertical and radial directions.

The load carrying capacity of deep-mixed cement columns was investigated using a finite element mesh extending 5D in the radial direction and 18D in the vertical direction, where D is the diameter of the deep-mixed cement column. During this analysis, the load carrying capacity of the columns was investigated for different degrees of cementation by varying the length to diameter ratio of the cement columns. The boundaries of the finite element mesh were constrained similarly to the footing analysis.

3 PARAMETERS DEFINING IN SITU AND CEMENTED SOIL BEHAVIOUR

The cemented soil model developed by Liu *et al.* (2006) is also developed within the Structured Cam Clay model framework (Liu and Carter, 2002). It uses five parameters to define the soil structure due to cementation, in addition to the usual parameters used to define destructured, reconstituted soil behaviour in the Modified Cam Clay model (Roscoe and Burland, 1968). The additional parameters are b, p'_{yi}, ω, γ, s_u, and they are described in the following paragraphs.

The destructuring index, b, quantifies the rate of de-structuring with increasing mean effective stress and p'_{yi} defines the mean effective yield stress at which the breakdown of the cemented structure begins. The two model parameters ω and γ define, respectively, the influence of soil structure due to cementation on the plastic potential of the soil and the effect of shearing on destructuring. The latter is directly proportional to the value of γ. As illustrated in Figure 1, an additional change in void ratio, Δe_i, is sustained by the cemented soil with respect to the reconstituted soil and is defined by:

$$e = e^* + \Delta e_i \left[\frac{p'_{yi} + C/M^*}{\overline{p}'} \right]^b \quad (1)$$

where e is the void ratio of the cemented soil, e^* is the void ratio of the same soil at the reconstituted state, and M^* is the critical state strength parameter of the soil without any cementation.

The degree of cementation has been incorporated in the cemented clay model by defining a modified effective stress parameter as:

$$\overline{p}' = p' + C/M^* \quad (2)$$

where $C = s_u/2$ and s_u is the undrained shear strength of the cemented soil. The parameter C incorporates the contribution of cementation to the shear strength of the soil with respect to the reconstituted soil.

The typical variation of void ratio, *e*, with the mean effective stress, p', for a cemented clay and for the same soil at the reconstituted state are illustrated in Figure 1. Figure 2 illustrates the yield surface for the cemented clay in p' – q stress space, which is given by:

$$F = q^2 + M^{*2}\overline{p}'(\overline{p}' - p'_s) \quad (3)$$

where p'_s is the size of the yield surface. The initial mean effective yield stress, p'_{yi}, is related to the size of the initial yield surface as follows:

$$p'_{si} = p'_{yi} + C/M^* \quad (4)$$

Although the yield surface for the cemented clay is elliptical, it does not pass through the origin in p' – q space. Non-associated plastic flow is assumed for the cemented soil (details are provided in the Appendix).

The Appendix to this paper provides a derivation of the incremental stress-strain matrix for the cemented clay model. This matrix is required in the finite element formulation where the model is used to solve boundary value problems such as those described later in this paper.

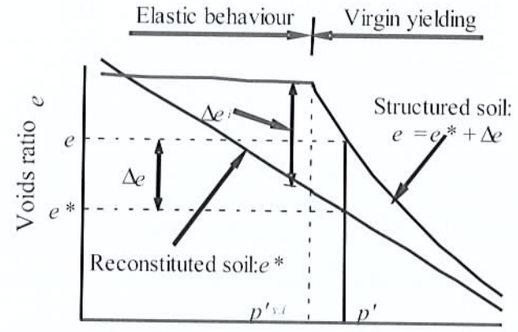

Figure 1. Compression behaviour of cemented soils

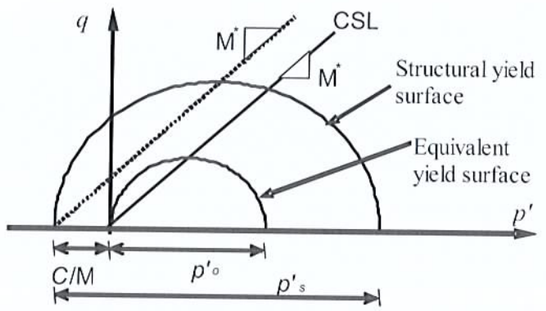

Figure. 2 Structural and equivalent yield surfaces for cemented clays

4 SOIL PARAMETERS

For the numerical results presented in this paper, cemented Ariake soil with cement contents of 6%, 9% and 12% have been considered. The cement content, A_w, is defined here as the ratio of cement to clay by dry mass.

The undisturbed soil around the cemented soil also has a structure and hence it was modelled using the Structured Cam Clay model (Carter and Liu, 2005). In order to obtain the properties of the cemented and undisturbed Ariake Clay, triaxial test results given by Horpibulsuk *et al.* (2004) have been used, and the derived values of the model parameters are presented in Table 1.

Table 1. Model parameters for undisturbed and cemented Ariake clay.

Property	Cement content			
	A_w = 0% (Undisturbed)	A_w = 6%	A_w = 9%	A_w = 12%
λ^*	0.43	0.43	0.43	0.43
κ^*	0.015	0.015	0.015	0.015
M^*	1.5	1.5	1.5	1.5
ν^*	0.25	0.25	0.25	0.25
e^*_{cs}	4.0	4.0	4.0	4.0
B	0.8	0.8	0.8	0.8
Δe_i	1.44	1.32	2.26	2.42
γ	0.02	0.02	0.02	0.02
ω	0.1	0.1	0.1	0.1
γ_b (kN/m^3)	17.0	17.0	17.0	17.0
p'_y (kN/m^2)	38.0	60.0	220.0	380.0
C (kN/m^2)	0.0	13.64	50.0	86.365
s_u (kN/m^2)		27.27	100.0	172.73

λ^* = gradient of the normal compression line in e – ln (p′) space,
κ^* = gradient of the unloading and reloading line in e – ln (p′) space,
M^* = gradient of the CSL in p′ - q space,
ν^* = Poisson's ratio,
e^*_{cs} = void ratio at p′ = 1 kPa on the CSL in e - ln (p′) space,
γ_b = bulk unit weight

Based on laboratory test results, Horpibulsuk *et al.* (2004, 2005) were able to relate the mean effective yield stress, p'_{yi}, and the undrained shear strength of the soil, s_u, by the following equation:

$$p'_{yi} = 2.2 s_u \quad (5)$$

During an *in situ* cement mixing process, a column of soil is cut by rotating blades and cement slurry or powder is forced into the ground while mechanically mixing it with the soil. Therefore the natural structure of the *in situ* soil will be highly disturbed during the deep cement mixing process, and will be replaced by a new structure due to the presence of the hydrated cement. It should be recognised that the five parameters defining soil structure will not, in general, be the same for the cemented soil and the undisturbed *in situ* soil. Unfortunately, the available data are not sufficient to assess all five parameters defining the soil structure for different degrees of cementation. Therefore, only Δe_i and p'_{yi} have been changed, with C for the different degrees of cementation considered in the finite element analyses carried out in what follows. It is assumed that parameters b, ω, and γ take the same values as for the *in situ* (undisturbed) Ariake clay without any cementation All properties describing the soil in its reconstituted states are the same for both the cemented and *in situ* Ariake clay and are denoted by the superscript *. Further details of this model have been given previously by Liu *et al.* (2006).

A number of other assumptions have been made in the process of choosing parameters for the cemented Ariake clay. In the cemented clay model it is assumed that the gradient of the critical state line, M^*, which is a function of the critical state friction angle of the soil, is the same as that of the Ariake clay at the reconstituted state. According to Horpibulsuk *et al.* (2004), the introduction of a small amount of cementation to the clay will increase the friction angle of the soil. However, they showed that this enhancement is insignificant with further increase in degree of cementation. Although the destructuring index, b, which controls the rate of breakage of cementation, is expected to vary with the cement content, the available data are insufficient to assess this variation. Therefore, the same value of b has been used for both undisturbed and cemented Ariake clay. In what follows, all properties of the destructured, reconstituted soil are denoted by the superscript *.

5 MODE OF BEARING CAPACITY FAILURE

Figures 3 (a) and (b) show respectively the cumulative soil displacements predicted beneath a 2.5 m diameter shallow footing on Ariake clay with cement contents of 6% and 12%. In both cases, displacement vectors represent the soil flow when the mobilised bearing resistance reaches the peak value. It can be seen that the failure mechanisms are not the same for the two cases considered. When the cement content is 6%, soil beneath the centre of the footing moves predominantly in the vertical direction, but towards the outer edge of the footing soil movement is predominantly in the radial direction and the soil heaves around the footing, similar to a general shear failure. For a cement content of 12% a similar pattern can be seen beneath the footing, but the displacement vectors closer to the edge of the footing are predominantly in the radial direction. They do not indicate heave of the ground surface, but rather a local shear failure.

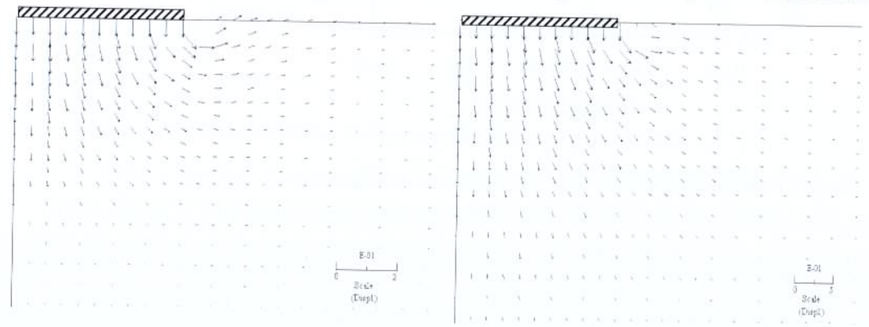

Figure 3. Cumulative displacements at peak bearing capacity (a) A_w = 6% and (b) A_w = 12%.

6 INFLUENCE OF CEMENT CONTENT ON BEARING CAPACITY

Figure 4 illustrates the predicted undrained bearing response of a 2.5 m diameter circular footing founded on Ariake clay with a cement content of 9%, which shows clearly that the mobilised bearing resistance reaches a peak value during undrained loading but beyond the peak starts to decrease gradually.

This behaviour can be explained by observing the stress path at a typical Gauss integration point located beneath the footing, as illustrated in Figure 5. Close to the ground surface, the initial effective stress of the soil is very low and therefore the cemented clay has a high over-consolidation ratio. Thus the undrained stress path rises approximately vertically on this plot. When the stress state reaches the structural yield surface of the cemented soil, it behaves as a virgin yielding material and the stress state moves approximately along the yield surface. Once $q/(p' + C/M^*)$ reaches M^* the process of destructuring begins. During this phase, resistance to shear deformation is reduced considerably and breakdown of soil structure begins, together with the removal of the effects of cementation. The behaviour of the soil element, particularly the undrained effective stress path shown in Figure 5, is consistent with experimental observations for highly over-consolidated soils (e.g., Bergado *et al.*, 2004; Horpibulsuk *et al.*, 2004). Thus the fundamental features of cemented clay seen in single element tests have been captured successfully in the numerical scheme when applied to a boundary value problem.

In the plot of bearing capacity versus displacement shown in Figure 4, this phase is marked by a decrease in the mobilised bearing resistance of the footing. Such decreases in the bearing resistance should be considered in geotechnical engineering designs if post-peak displacement is allowed to occur for a practical structure.

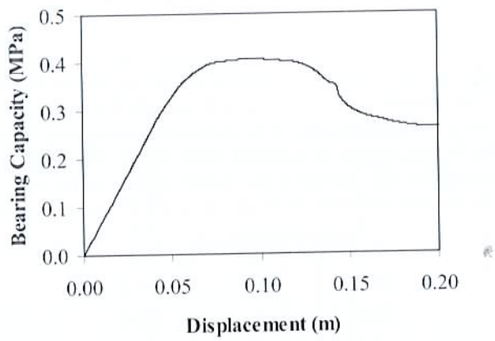

Figure 4. Predicted undrained bearing capacity for a 2.5 m diameter circular footing (A_w = 9%)

With increase in the degree of cementation, A_w, the mobilised bearing resistance increases significantly, as illustrated in Figure 6. For example, when A_w = 9%, there is a five-fold increase in the predicted maximum mobilised bearing resistance, compared to the undrained bearing resistance obtained for the natural undisturbed soil with A_w = 0%.

Figure 5. Stress path at a Gauss integration point beneath the footing.

The dependency of the elastic deformation parameters of soils on cementation and sub-yielding behaviour has been observed experimentally by Miura *et al.* (2001), Bergado *et al.* (2004) and Horpibulsuk *et al.* (2004). However, the constitutive model used for this study assumes that the behaviour of both cemented and uncemented clays is independent of cementation for loading inside the yield surface. Although this is a limitation of the current cemented clay model, it can still capture the important facets of cemented clay behaviour during loading, such as the destructuring phase of the cemented clay, which contribute to the reduction in peak bearing resistance during loading.

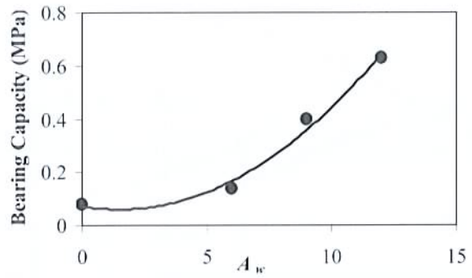

Figure 6. Variation of undrained bearing capacity with degree of cementation.

7 INFLUENCE OF THE SIZE OF CEMENTED ZONE ON BEARING CAPACITY

Figure 7 shows the influence of the depth of the cemented region, H, on the bearing capacity of the foundation. The cement content of the soil is 9% and the diameter, B, of the footing considered for the analysis is 2.5 m. The case with H/B = 0 corresponds to the soil without any cementation. For the results shown in Figures 6 and 7, the depth of the cement-improved region changed while keeping the width of the cement improved region constant to the full width of the finite element mesh. It can be seen that even a thin layer of cemented soil beneath the footing can have a significant influence on the mobilized bearing resistance. For example, a two-fold increase in bearing capacity is observed with just a 0.25 m thick layer (H/B = 0.1) of cemented soil beneath the footing.

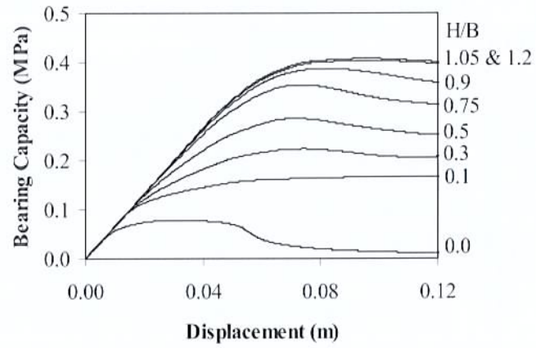

Figure 7. Variation of bearing capacity with the depth of the cemented region.

Figure 8 shows the bearing capacity improvement factor defined as q_u(cemented)/q_u(uncemented) for different H/B, and it shows clearly the influence of H/B on the maximum bearing capacity. This figure corresponds to A_w = 9% and it can be seen that the bearing capacity of the footing increases up to H/B = 1, but beyond this limit further increase in the depth of cemented region H does not have a significant influence on the maximum bearing capacity. Again, a five-fold increase in bearing capacity could be achieved for A_w = 9% when H/B = 1.

experimental results given by Horpibulsuk *et al.* (2004, 2005) for cemented Ariake clay. The failure modes studied for different degrees of cementation suggest that when the cement content is about 12% failure occurs similar to a local shear failure, and for lower cement content failure occurs as a general shear failure. In both failure modes, the mobilised bearing resistance decreases after reaching the peak due to breakage of the cement structure. Although significant ground heave could be seen around the footing for low cement contents (A_w = 6% and 9%), with increase in cement soil heaving around the footing is suppressed.

The parametric study shows that the influence of cementation significantly increases the mobilised bearing resistance of footings. It was found that there is an effective region for the application of deep cement mixing with respect to the footing size but the size of this region is independent of the cement content.

Numerical studies were carried out to study the load-displacement response of deep cement-mixed columns and the results suggest that there is an optimum L/D ratio based on the cement content and by increasing L beyond the optimum value, the load carrying capacity of the column cannot be increased.

10 REFERENCES

Bergado, D.T., Lorenzo, G.A. and Abdul-Naga, H.H. (2004). Fundamentals of thermal and cements stabilisation, *Proceedings of the Inernational. Symposium on Lowland Technology*, Plenary session and Keynote lectures, pp. 23-40.

Carter, J.P. and Balaam, N.P. (1995). *AFENA User Manual*, Version 6, University of Sydney.

Carter, J.P. and Liu, M.D. (2005). Review of the Structured Cam Clay model, *Soil constitutive models: evaluation, selection, and calibration*, ASCE, Geotechnical special publication No. 128, pp. 99-132.

Dong, P., Qin, R. and Chen, Z. (2004). Bearing capacity and settlement of concrete-cored DCM pile in soft ground, *Geotechnical and Geological Engineering*, Vol. 22, pp. 105-119.

Han, J. and Gabr, M.A. (2002). Numerical analysis of geosynthetic-reinforced and pile-supported earth platforms over soft soil, *Journal of Geotechnical and Geoenvironmental Engineering*, Vol. 128, No. 1, pp. 44-53.

Horpibulsuk, S., Miura, N. and Bergado, D.T. (2004). Undrained shear behaviour of cement admixed clay at high water content. *Journal of Geotechnical and Geoenvironmental Engineering*, ASCE, Vol. 130, No. 10, pp. 1096-1105.

Horpibulsuk, S., Miura, N. and Nagaraj, T.S. (2005). Clay-water/cement ratio identity for cement admixed soft clays. *Journal of Geotechnical and Geoenvironmental Engineering*, ASCE, Vol. 131, No. 2, pp. 187-192.

Kamon, M. and Bergado, D.T. (1991). Ground improvement techniques, *Proceedings of the Ninth Asian Regional Conference of Soil Mechanics and Foundation Engineering*, Bangkok, Thailand, Vol. 2, pp. 526-546.

Kasama, K., Ochiaia, H. and Yasufuku, N. (2000). On the stress-strain behaviour of lightly cemented clay based on an extended critical state concept, *Soils and Foundations*, Vol. 40, No. 5, pp. 37-47.

Liu, M. D. and Carter, J. P. (2002), "Structured Cam Clay Model", *Canadian Geotechnical J.* Vol. 39(6), 1313-1332.

Liu, M. D., Carter, J. P., Horpibulsuk, S. and Liyanapathirana, D.S. (2006), "Modelling the behaviour of cemented clay.", *Geotechnical Special Publication No. 152,* pp. 65-72

Liyanapathirana, D.S., Carter, J.P. and Airey, D.W. (2005). Numerical modeling of nonhomogeneous behaviour of structured soils during triaxial tests, *International Journal of Geomechanics*, ASCE, Vol. 5, No. 1, pp. 10-23.

Liyanapathirana, D.S. and Carter, J.P. (2005). Undrained bearing capacity of shallow foundations on structured soils. In Proceedings, *International Symposium on Frontiers in Offshore Geotechnics*, Perth, Australia, 19-21 September, pp. 451-457.

Liyanapathirana, D.S., Liu, M.D., Airey, D.W. and Carter, J.P. (2003a). Predicting the behaviour of foundations on structured soils. In Proceedings, *XIIIth European Conference on Soil Mechanics and Geotechnical Engineering*, Prague, Czech Republic, 25-28 August, Vol.2, pp. 255-260.

Liyanapathirana, D.S., Carter, J.P. and Airey, D.W. (2003b). Bearing response of shallow foundations on structured soils. In Proceedings, *International Conference on Foundations: Innovations, Observations, Design and Practice*, Dundee, Scotland, 2-5 September, pp. 521-530.

Miura, N., Horpibulsuk, S. and Nagaraj, T.S. (2001). Engineering behaviour of cement stabilised clay at high water content, *Soils and Foundations*, Vol. 41, No. 5, pp. 33-45.

APPENDIX – INCREMENTAL STRESS-STRAIN MATRIX FOR CEMENTED CLAY

The derivation of the incremental stress-strain matrix for the cemented clay model is presented in this Appendix. The yield surface of the cemented clay, defined by $F(\sigma', \varepsilon_v^p) = 0$, depends on the stress state and the plastic volumetric strain. Hence, an incremental change in the yield function (Equation 3) is given by:

$$dF = \left\{\frac{\partial F}{\partial \sigma'}\right\}^T \{d\sigma'\} + \frac{\partial F}{\partial \varepsilon_v^p} d\varepsilon_v^p = \left\{\frac{\partial F}{\partial \sigma'}\right\}^T \{d\sigma'\} + \frac{\partial F}{\partial \varepsilon_v^p} [N]\{d\varepsilon^p\} = 0 \quad (6)$$

where $d\varepsilon_v^p$ is the increment in plastic volumetric strain and $\{d\sigma'\}$ and $\{d\varepsilon^p\}$ are, respectively, the corresponding increments in the stress state and plastic strain of the soil. Since the problem is axisymmetric, $\{d\sigma'\}$ is given by:

$$\{d\sigma'\} = \begin{Bmatrix} d\sigma_r' \\ d\sigma_z' \\ d\sigma_\theta' \\ d\tau_{rz} \end{Bmatrix} \quad (7)$$

where $d\sigma_r'$, $d\sigma_z'$ and $d\sigma_\theta'$ are respectively, the radial, vertical and tangential components of the effective stress increment and $d\tau_{rz}$ is the increment in shear stress, and

$$[N] = \begin{bmatrix} 1 & 0 & 0 & 0 \\ 0 & 1 & 0 & 0 \\ 0 & 0 & 1 & 0 \\ 0 & 0 & 0 & 0 \end{bmatrix} \quad (8)$$

Although strains will contain both elastic and plastic components, only elastic strains can generate stresses through the elastic constitutive matrix [D]. Therefore, the change in stress state is given by:

$$\{d\sigma'\} = [D](\{d\varepsilon\} - \{d\varepsilon^p\}) = ([D] - [D_p])\{d\varepsilon\} \quad (9)$$

where $[D_p]$ is the plastic constitutive matrix and $\{d\varepsilon\}$ is the increment in total strain. The increment in plastic strain, $\{d\varepsilon^p\}$, is given by:

$$\{d\varepsilon^p\} = \Lambda \left\{\frac{\partial G}{\partial \sigma'}\right\} \quad (10)$$

where Λ is a plastic scaling factor and G is the plastic potential function. For the cemented clay model, non-associated plastic flow is assumed. Therefore, the plastic potential, G, is different from the yield function, F. By substituting Equations (8) to (10) in (6), the plastic scaling factor can be obtained as:

$$\Lambda = \frac{\left\{\frac{\partial F}{\partial \sigma'}\right\}^T [D]\{d\varepsilon\}}{\left\{\frac{\partial F}{\partial \sigma'}\right\}^T [D]\left\{\frac{\partial G}{\partial \sigma'}\right\} - \frac{\partial F}{\partial \varepsilon_v^p}[N]\left\{\frac{\partial G}{\partial \sigma'}\right\}} \quad (11)$$

From Equation (9), the plastic constitutive matrix $[D_p]$ can then be obtained as:

$$[D_p] = \frac{[D]\left\{\frac{\partial G}{\partial \sigma'}\right\}^T \left\{\frac{\partial F}{\partial \sigma'}\right\}[D]}{\left\{\frac{\partial F}{\partial \sigma'}\right\}^T [D]\left\{\frac{\partial G}{\partial \sigma'}\right\} - \frac{\partial F}{\partial \varepsilon_v^p}[N]\left\{\frac{\partial G}{\partial \sigma'}\right\}} \quad (12)$$

To obtain the plastic constitutive matrix $[D_p]$ for the structured soil, appropriate expressions for $\left\{\frac{\partial F}{\partial \sigma'}\right\}$, $\left\{\frac{\partial G}{\partial \sigma'}\right\}$, $[D]$ and $\frac{\partial F}{\partial \varepsilon_v^p}$ should be substituted in Equation (12). Further details are provided as follows for the cemented clay model.

In an axi-symmetric coordinate system, the elastic behaviour of the cemented clay is described by:

$$[D]=\begin{bmatrix} K+\frac{4}{3}\mu & K-\frac{2}{3}\mu & K-\frac{2}{3}\mu & 0 \\ K-\frac{2}{3}\mu & K+\frac{4}{3}\mu & K-\frac{2}{3}\mu & 0 \\ K-\frac{2}{3}\mu & K-\frac{2}{3}\mu & K+\frac{4}{3}\mu & 0 \\ 0 & 0 & 0 & \mu \end{bmatrix} \quad (13)$$

where the elasticity coefficients are define as:

$$K=\frac{(1+e)p'}{\kappa^*} \quad (14)$$

$$\mu=\frac{3(1-2\nu^*)}{2(1+\nu^*)}K \quad (15)$$

where ν^* is Poisson's ratio of the soil skeleton, K and μ are the elastic bulk and shear moduli, respectively, e is the current voids ratio of the soil and p′ is the mean effective stress.

An increment in the plastic volumetric strain, $d\varepsilon_v^p$, can only occur with a change in the yield surface, controlled by p_s'. Hence, $\partial F/\partial \varepsilon_v^p$ can be written as:

$$\frac{\partial F}{\partial \varepsilon_v^p}=\frac{\partial F}{\partial p_s'}\frac{\partial p_s'}{\partial \varepsilon_v^p} \quad (16)$$

According to Liu *et al.* (2006), the increment in plastic volumetric strain of a cemented soil is given by:

$$d\varepsilon_v^p=(\lambda^*-\kappa^*)\frac{dp_s'}{(1+e)p_s'}+b\left(\langle\Delta e\rangle+\frac{\gamma\overline{\eta}\Delta e}{M^*-\overline{\eta}}\right)\frac{dp_s'}{(1+e)p_s'} \quad (17)$$

$$\langle\Delta e\rangle=\begin{cases}\Delta e \text{ if } |\Delta e|\geq 0\\ 0 \text{ if } |\Delta e|<0\end{cases} \quad (18)$$

where $\overline{\eta}$ is the ratio between deviatoric stress and the modified mean effective stress, $\overline{p}'$. λ^* and κ^* are, respectively, the gradients of normal compression and, unloading and reloading lines of the reconstituted soil in e-ln(p′) space, e is the void ratio of the cemented soil and Δe is the difference in void ratio between the cemented soil and the corresponding reconstituted soil at the same stress state, e^*.

From Equation (3), $\partial F/\partial p_s'$ can be derived as:

$$\frac{\partial F}{\partial p_s'}=-M^{*2}\overline{p}' \quad (19)$$

By substituting Equations (17) and (19) into Equation (16) it is found that:

$$\frac{\partial F}{\partial \varepsilon_v^p}=\frac{(-M^{*2}\overline{p}')(1+e)p_s'}{\left((\lambda^*-\kappa^*)+b\left(\langle\Delta e-c\rangle+\frac{\gamma\overline{\eta}}{M^*-\overline{\eta}}\right)\right)} \quad (20)$$

The stress gradients of the yield function, $\left\{\frac{\partial F}{\partial \sigma'}\right\}$, can be calculated from:

$$\left\{\frac{\partial F}{\partial \sigma'}\right\}=\begin{Bmatrix}\frac{\partial F}{\partial p'}\frac{\partial p'}{\partial \sigma_r'}+\frac{\partial F}{\partial q}\frac{\partial q}{\partial \sigma_r'}\\ \frac{\partial F}{\partial p'}\frac{\partial p'}{\partial \sigma_z'}+\frac{\partial F}{\partial q}\frac{\partial q}{\partial \sigma_z'}\\ \frac{\partial F}{\partial p'}\frac{\partial p'}{\partial \sigma_\theta'}+\frac{\partial F}{\partial q}\frac{\partial q}{\partial \sigma_\theta'}\\ \frac{\partial F}{\partial q}\frac{\partial q}{\partial \tau_{rz}}\end{Bmatrix} \quad (21)$$

where

$$p'=\frac{(\sigma_r'+\sigma_z'+\sigma_\theta')}{3} \quad (22)$$

and

$$q=\frac{1}{\sqrt{2}}\left((\sigma_r'-\sigma_z')^2+(\sigma_z'-\sigma_\theta')^2+(\sigma_\theta'-\sigma_r')^2+6\tau_{rz}^2\right)^{1/2} \quad (23)$$

For an eliptical yield surface (Equation 3), the stress gradients of the yield function are given by:

$$\frac{\partial F}{\partial p'}=\frac{\partial F}{\partial \overline{p}'}=M^{*2}(2\overline{p}'-p_s') \quad (24)$$

and

$$\frac{\partial F}{\partial q}=2q \quad (25)$$

The gradients of the stress invariants p′ and q are defined as:

$$\frac{\partial p'}{\partial \sigma_r'}=\frac{\partial p'}{\partial \sigma_\theta'}=\frac{\partial p'}{\partial \sigma_z'}=\frac{1}{3} \quad (26a)$$

$$\frac{\partial q}{\partial \sigma_r'}=\frac{2\sigma_r'-\sigma_z'-\sigma_\theta'}{2q} \quad (26b)$$

$$\frac{\partial q}{\partial \sigma_z'}=\frac{2\sigma_z'-\sigma_r'-\sigma_\theta'}{2q} \quad (26c)$$

$$\frac{\partial q}{\partial \sigma_\theta'}=\frac{2\sigma_\theta'-\sigma_z'-\sigma_r'}{2q} \quad (26d)$$

The vector $\left\{\frac{\partial G}{\partial \sigma'}\right\}$ can be obtained by substituting the plastic potential function, G, instead of the yield function, F, in Equation (21). Although G itself is unknown, $\frac{\partial G}{\partial p'}$ and $\frac{\partial G}{\partial q}$ can be found as they are proportional respectively to the increment in plastic volumetric strain, $d\varepsilon_v^p$, given by Equation (17), and the increment in plastic deviatoric strain, $d\varepsilon_d^p$, given by (Liu *et al.*, 2006):

$$d\varepsilon_d^p=\frac{2\overline{\eta}}{\left|M^{*2}-\overline{\eta}^2\right|+\omega\left|1-\sqrt{\frac{p_o'}{p_s'}}\right|}\times\left\{(\lambda^*-\kappa^*)+b\left[\langle\Delta e\rangle+\left[1+\frac{\gamma\overline{\eta}\Delta e}{M^*-\overline{\eta}}\right]\right]\right\}\frac{dp_s'}{(1+e)p_s'} \quad (27)$$

p'_o is the size of the equivalent yield surface, as shown in Figure 2, which passess through the origin of the p' - q space and which is given by (Liu *et al.*, 2006):

$$p'_o = \frac{e^{\frac{e_{IC}}{\lambda^* - \kappa^*}}}{p'^{\frac{\kappa^*}{\lambda^* - \kappa^*}}} \tag{28}$$

p'_o represents the size of the yield surface for the reconstituted soil at the same stress state and same voids ratio.

The increment in plastic deviatoric strain is not the same for all stress states of the cemented clay. Equation (27) is valid when $\overline{\eta} < M^*$. However, when the stress state passes the Critical State Line, where $\overline{\eta} > M^*$, the soil starts to soften. During the softening process, volumetric deformation is defined using the same equation (Equation 17), but the deviatoric strain increment is modified to ensure that the deviatoric deformation due to destructuring has the same sign as soil at the reconstituted state (Liu *et al.*, 2006), i.e.,

$$d\varepsilon_d^p = \frac{2\overline{\eta}}{\left|M^{*2} - \overline{\eta}^2\right| + \omega\left|1 - \sqrt{\frac{p'_o}{p'_s}}\right|} \times \left[\left(\lambda^* - \kappa^*\right) + \frac{\gamma\overline{\eta}\, b\Delta e}{M^* - \overline{\eta}}\right] \frac{dp'_s}{(1+e)p'_s} \tag{29}$$

During virgin yielding, soil can reach a stress state with $\overline{\eta} = M^*$ and $\Delta e \neq 0$ before reaching the critical state of deformation. In this situation, soil structure due to cementation will rearrange, with crushing of the cemented structure, until the soil reaches its final critical state of deformation. During this process, the stress state must move up or down the CSL, depending on whether the soil is hardening or softening, respectively, and the plastic constitutive matrix for the incremental finite element analysis is derived using the relationship for plastic volumetric strain increment given by Equation (17). As suggested by Liu *et al.* (2006), the following relationship is adopted for this type of plastic deviatoric deformation:

$$d\varepsilon_d^p = \frac{2\overline{\eta}\left|d\varepsilon_v^p\right|}{\omega\left(1 - 2\nu^*\right)\left|1 - \sqrt{p'_o / p'_s}\right|} \tag{30}$$

To obtain the breakdown of the cementation in cemented Ariake clay beyond the peak strength state reached during loading, Liu et al. (2006) proposed the following empirical equation based on the experimental results:

$$dC = -\left[\left(\frac{q}{p'}\right)^3 - M^{*3}\right]\left|dp'\right| \tag{31}$$

This Appendix has provided only the equations relevant for the finite element formulation of the cemented clay model, based on cemented Ariake clay. A more detailed discussion of the model and derivation of the constitutive relations are given by Liu *et al.* (2006). Liu *et al.* (2006) simulated the conventional triaxial tests carried out by Horpibulsuk *et al.* (2005) at different levels of confining pressures using the cemented clay model and showed that this model is capable of predicting well the experimentally observed behaviour of cemented Ariake clay.